JREE: Vol. 12, No. 4, (Autumn 2025) 29-39

Journal of Renewable Energy and Environment

Journal Homepage: www.jree.ir

Materials and Energy Research Center

MERC

Research Article

Experimental Analysis and Modeling of the Collector And Absorber Temperatures of the Solar Chimney as a Function of Solar Radiation, Ambient Temperature, and Position

Razika Ihaddadene[a,b]*, Ammar Semane[a,c], Nabila Ihaddadene[a,b], Elhouas Bedjeghit[a,b], Belhi Guerira[d]

[a] Department of Mechanical Engineering, Faculty of Tehnnology, University of M'sila, P. O. Box: 28000, M'sila, Algeria.
[b] Laboratory of Water, Environment and Renewable Energies, University of M'sila, P. O. Box: 28000, M'sila, Algeria.
[c] Laboratory of Materials and Mechanics of Structures (L.M.M.S), University of M'sila, P. O. Box: 28000, M'sila, Algeria.
[d] Laboratory of Mechanical Engineering L.M.G, University of Mohamed Khider, Biskra, Algeria.

PAPER INFO

Paper history:
Received: 13 January 2025
Revised: 19 June 2025
Accepted: 22 September 2025

Keywords:
Sola Chimney,
Absorber Temperature,
Collector Temperatur,
Solar Radiation,
Raduim,
Mathemathecal Models

ABSTRACT

The solar chimney is an innovative technology that harnesses solar energy to generate electricity sustainably. This experimental study presents a modeling approach for predicting collector and absorber temperatures in a small solar chimney prototype. Temperatures were measured at five positions on the collector and absorber under varying solar radiation and ambient conditions. The results demonstrate that local temperatures at each position can be accurately represented by a second-order polynomial regression of solar radiation and ambient temperature, with R^2 values ranging from 0.973 to 0.989 for the collector and from 0.9619 to 0.9835 for the absorber. A key innovation of this work is the generalization of these local models into a unified thermal model capable of predicting temperatures at any point on the collector or absorber surface. This was achieved by expressing the regression coefficients of the local models as fourth-order polynomial functions of the radial position. Model validation using statistical indices—including R^2, RMSE, NRMSE, and NSE—demonstrated strong agreement with experimental data. For the absorber, $R^2 = 0.974$, NRMSE = 0.0174, and NSE = 0.974; for the collector, $R^2 = 0.9802$, NRMSE = 0.0194, and NSE = 0.98. These results confirm the accuracy of the generalized model, providing a practical tool for simulating thermal fields in solar chimneys and optimizing system performance with reduced experimental effort.

https://doi.org/10.30501/jree.2025.497013.2217

1. INTRODUCTION

The utilization of renewable energy has gained increasing attention as an alternative to fossil fuels. Unlike fossil fuels, which are finite and highly polluting, renewable energy sources—including solar, wind, hydroelectric, and geothermal—are inexhaustible and produce little to no greenhouse gas emissions. By relying on these sources, it is possible to significantly reduce environmental impact, decrease dependence on imported fossil fuels, and contribute to mitigating global warming. Furthermore, renewable energy fosters local job creation and drives technological innovation, supporting a sustainable energy transition and a greener economy.

Renewable energy is playing an increasingly important role in global electricity generation. According to the International Energy Agency (IEA) (irena et al, 2024), approximately 30% of the world's electricity was generated from renewable sources in 2022, a share that continues to rise due to the rapid growth of solar and wind technologies. In Europe, renewables surpassed fossil fuels for the first time in 2020, accounting for around 38% of total electricity production (ec.europa,2024). China has emerged as the world's largest producer of solar and wind energy, installing more than half of the global capacity in both sectors in 2022 (irena et al, 2024). Solar and wind are the fastest-growing renewable sources, together representing over 80% of new installed capacity in 2021 (irena et al, 2024), with solar energy exhibiting an average annual growth of 22% over the past decade. In the first half of 2024, the EU generated more electricity from wind and solar than from fossil fuels (ember-energy,2024). Despite this rapid growth, challenges remain, particularly in energy storage and integration into electricity grids. Nevertheless, projections suggest that renewables could account for 50% of global electricity production by 2050, playing a central role in the energy transition.

The solar chimney is an emerging technology for electricity generation, complementary to photovoltaic systems, and consists of three primary components: the collector, the chimney, and the turbine. It combines the greenhouse effect and the buoyancy effect to generate electricity (Mamgain et al., 2021; Abuashe & Mariamy., 2024). With appropriate thermal storage, it has the potential to provide electricity continuously in regions with high solar intensity. The collector absorbs solar radiation, heating the air via the greenhouse effect, which then rises through the chimney, converting part of the thermal

*Corresponding Author's Email: azika.ihaddadene@univ-msila.dz (R. Ihaddadene)
URL: https://www.jree.ir/article_230102.html

Please cite this article as: Ihaddadene, R., Semane, A., Ihaddadene, N., Bedjeghit, E. & Guerira, B. (2025). Experimental Analysis and Modeling of the Collector And Absorber Temperatures of the Solar Chimney as a Function of Solar Radiation, Ambient Temperature, and Position. *Journal of Renewable Energy and Environment (JREE)*, 12(4), 29-39.- https://doi.org/10.30501/jree.2025.497013.2217.

energy into kinetic energy that drives a turbine. Despite its relatively simple operating principle and ease of construction, the technology faces challenges, particularly low efficiency. Various hybridization strategies have been proposed to improve performance, including the integration of geothermal energy (Mokrani et al., 2020), water desalination systems (Alksrawi et al.,2021,Sharon &Srinivas 2024), photovoltaic solar cells (Abdelsalam et al., 2023), waste heat systems (Habibollahzade et al., 2018), heat exchangers (Aliaga et al., 2021), and cooling towers (Zou & He, 2015). Solar chimney technology thus holds promise not only for electricity generation but also for producing hydrogen, desalinated water, and other hybrid energy applications (Abdelsalam et al., 2024).

The performance of solar chimneys is influenced by numerous parameters, which can be broadly classified into two categories: climatic parameters and geometric parameters. Climatic parameters relate to the installation site of the solar chimney and include solar radiation, ambient temperature, wind speed, and humidity. Several studies have investigated these factors (Dai et al., 2003, Semane et al., 2025, Laribi et al., 2010, Aydi et al., 2021, Setrah, 2021), consistently highlighting the dominant effects of solar radiation and ambient temperature. Solar radiation positively impacts solar chimney performance, as confirmed experimentally (Dai et al., 2003, Semane et al., 2025), mathematically (Laribi et al., 2010), and numerically (Aydi et al., 2021, Setrah, 2021). The influence of ambient temperature, however, remains debated: some studies report a positive effect (Laribi et al., 2010, Aydi et al., 2021), while others indicate a negative impact (Dai et al., 2003, Cuce et al.,2021a, Zhou et al., 2010).

Geometric parameters pertain to the dimensions and shape of the solar chimney, including the diameter and height of the collector and chimney, as well as their respective profiles (Ihaddadene et al., 2023, Karimipour-Fard & Beheshti, 2017, Yapici et al., 2020, Sen et al., 2021, Ayadi et al., 2018a, Hamdani, 2013, Ayadi et al., 2018b, Shahi et al., 2018, Cuce et al., 2021b, Kasaceia et al., 2014, Patel et al., 2014, Ghalamchi et al., 2016). Studies indicate that increasing the collector diameter enhances collector temperature, maximum airflow velocity, mass flow rate, power output, and efficiency, while increasing collector height negatively affects power output, efficiency, pressure, and temperature changes. Chimneys with larger diameters perform better, and increasing chimney height improves power output, mass flow, turbine pressure drop, and turbine input speed.

Large-scale solar chimneys require substantial space and advanced construction technology. Recently, Abuashe & Mariamy (2024) explored design modifications—such as reducing chimney diameter, incorporating helical collector paths, and adjusting virtual chimney height—to minimize overall dimensions, concluding that chimney height and collector diameter can be reduced by up to 83.58% and 25%, respectively. Such reductions enhance the feasibility of constructing solar chimney power plants using conventional structural technologies.

The design of collector and chimney convergence or divergence also affects performance. Divergent chimney shapes are generally reported as optimal, with researchers identifying specific divergent angles that maximize efficiency (Nasraoui et al., 2019, Hasan et al., 2018). Collector slope (positive or negative) influences airflow patterns, where excessive slopes can induce vortex formation, increasing losses and reducing efficiency. Moderate positive slopes, however, tend to enhance performance (Ayadi et al., 2018a, Cuce et al.,2021a, Patel et al., 2014, Ghalamchi et al., 2016, Cuce et al., 2024).

Previous experimental work (Semane et al., 2025) demonstrated that ambient temperature and solar radiation directly affect the average temperatures of the collector and absorber. These effects were quantified using mathematical models relating average absorber (or collector) temperature to both ambient temperature and solar radiation. Model validation employed the coefficient of determination and root mean square error. Additionally, average air temperature is influenced by collector and absorber temperatures, and a model was developed to describe this relationship (Ihaddadene et al., 2025). The temperature of the collector (or absorber) varies according to its radius, increasing as the radius decreases. Similarly, air temperature is inversely proportional to collector radius (Shuia et al., 2014, Ayad et al., 2015).

Most previous studies rely on numerical simulations, often fixing ambient temperature and solar radiation values, focusing primarily on airflow temperature. In contrast, the present work allows these variables to evolve dynamically in response to changing ambient conditions. Because collector and absorber temperatures directly affect air temperature and overall solar chimney performance, accurate modeling of these components is critical. This experimental study models the thermal behavior of the collector and absorber in a small solar chimney prototype, examining five locations on each component. Local models were developed using second-order polynomial regression with solar radiation and ambient temperature as predictors. A generalized model was then formulated by incorporating the positional variable, enabling prediction of collector and absorber temperatures based on three inputs: solar radiation, ambient temperature, and position. The models were validated using statistical indices including R^2, RMSE, NRMSE, and NSE.

This article is organized into four sections: an introduction; materials and methods, presenting the experimental setup and approach for developing generalized models; results and discussion; and a concluding section summarizing key findings.

2. EXPERIMENTAL

The objective of the experiment was to analyze the thermal behavior of the collector and absorber in a solar chimney under real-world conditions. Ambient temperature and solar radiation were measured alongside temperatures at five distinct locations on both the collector and absorber over the course of a day. These experimental data were subsequently used to develop and validate thermal models of the collector and absorber.

The experimental setup consisted of a solar chimney prototype, as shown in Figure 1. The collector has a diameter of 0.5 m and a height of 0.1 m, while the chimney height is 1 m. The collector, absorber, and chimney are constructed from steel, Plexiglas, and plastic, respectively.

Solar radiation and wind speed were measured using a hand pyranometer (489020) with a precision of ±5% and an anemometer (PCS X Wind Speed Sensor) with a precision of 0.1 m/s. Ambient temperature was recorded with a DS18B20 sensor, accurate to ±0.5 °C. Similar temperature sensors were positioned on the collector and absorber at five points each, labeled positions 1 through 5, spaced 10 cm apart along the radius, with radii of 48.75 cm (position 1), 38.75 cm (position 2), 28.75 cm (position 3), 18.75 cm (position 4), and 8.75 cm (position 5), as illustrated in Figure 1.

All temperature sensors were connected to an Arduino microcontroller, enabling real-time measurement of collector

and absorber temperatures. The pyranometer, anemometer, and ambient temperature sensor were also connected to the Arduino system to record solar radiation, wind speed, and ambient temperature. Data were automatically logged to an SD card at one-minute intervals.

The experiment was conducted at Mohamed Khider University in Biskra, Algeria (34°51′N, 5°44′E) on May 9, 2022. Throughout the day, variations in collector temperature (T_col) and absorber temperature (T_abs) at all five positions, ambient temperature (T_amb), solar radiation (G), and wind speed were continuously monitored to capture the thermal dynamics of the solar chimney under actual operating conditions.

Figure 1. Solar chimney prototype.

The expanded uncertainty of the temperature measurements was estimated at ±0.59 °C with a 95% confidence level. This accounts for the technical specifications of the DHT22 sensors, which have a stated accuracy of ±0.5 °C, as well as potential errors from analog-to-digital conversion, assumed to contribute ±0.1 °C of uncertainty.

3. THERMAL MODELING METHODOLOGY

This section describes the approach adopted to establish a mathematical model for predicting the collector (or absorber) temperature of the solar chimney as a function of ambient temperature, solar radiation, and spatial position on the collector (or absorber).

3.1 Purpose of the model

The objective is to develop a model capable of calculating the collector (or absorber) temperature at different positions along the system based on solar radiation, ambient temperature, and spatial location. This model enables interpretation of the overall thermal behavior of the system using experimental measurements.

3.2 Experimental data used

Measurements were collected at five distinct points distributed along the collector (or absorber) of the solar chimney. For each point, the temperature was recorded simultaneously with the corresponding solar radiation (G) and ambient temperature (T_amb). These data formed a comprehensive database for model development.

3.3 Local mathematical model

For each position i on the collector (or absorber), the temperature Ti was modeled as a second-order polynomial function of solar radiation G and ambient temperature T_{amb} as expressed below:

$$T_i = a \times G^2 + b \times G + c \times T_{amb}{}^2 + d \times T_{amb} + e \quad (1)$$

where the coefficients a, b, c, d, and e are specific to each position. This formulation accounts for the nonlinear effects associated with climatic variations.

3.4 Generalization of the model by position

The coefficients of the local models vary depending on the position along the collector (or absorber). To construct a global model, each coefficient is expressed as a fourth-order polynomial function of the spatial position x. For example, the coefficient a(x) is represented as:

$$a(x) = a_0 + a_1 \times x + a_2 \times x^2 + a_3 \times x^3 + a_4 \times x^4 \quad (2)$$

The other coefficients ((b (x), c (x), d (x), e (x)) can be similarly calculated. Thus, the temperature at point x on the collector (or absorber) is written in the form:

$$T_{col(abs)}(x) = a_{col/abs}(x) \times G^2 + b_{col/abs}(x) \times G + c_{col/abs}(x) \times T_{amb}{}^2 + d_{col/abs}(x) \times T_{amb} + e_{col/abs}(x) \quad (3)$$

This generalized model makes it possible to predict the temperature at any position x on the collector (or on absorber).

3.5 hypotheses

- The thermal properties of the collector (or absorber) are assumed to remain constant over time.
- The effects of wind and other environmental factors are considered negligible.
- The measurements are assumed to represent stable operating conditions.

The resulting generalized model was subsequently validated using experimental data, as described in the following section..

4. RESULTS AND DISCUSSION

Before presenting the results, the modeling approach adopted in this study is described. First, the effects of climatic conditions—ambient temperature and solar radiation—on the collector (or absorber) temperature were analyzed separately. When both temperature and radiation were found to influence the collector (or absorber) temperature, a predictive model was developed using a two-level polynomial approach. The first level involved local modeling of the temperature at five distinct points as a function of ambient temperature and solar radiation. In the second level, the coefficients obtained from the local models were generalized as functions of spatial position. This methodology allows the development of a global model capable of predicting the collector (or absorber) temperature as a function of ambient temperature, solar radiation, and position on the collector.

4.1 Evolution of the collector and aorber temperature as a function of raduis

The collector temperature (T_{col}) and absorber temperature (T_{abs}) are influenced by their respective radial positions as well as temporal factors, including solar radiation and ambient temperature. Both temperatures decrease proportionally with increasing radius of the collector or absorber. For example, at 13:10 P.M., under solar radiation of 941.82 W/m², ambient temperature of 30.44 °C, and wind velocity of 2.23 m/s, the

collector temperature decreases as the radius R increases, as illustrated in Figure 2(a). Specifically, T_{col} was 46.93 °C at point 4 (D=18.75D = 18.75D=18.75 cm), while it was 44.39 °C at point 2 (D=38.75D = 38.75D=38.75 cm). This 20 cm increase in radius corresponds to a 2.54 °C drop in temperature, representing a 5.41% relative decrease. The linear temperature decrease with radius is characterized by a coefficient of determination $R^2 = 0.929$ and can be expressed mathematically as follows:

$$T_{col}(R) = -0{,}0986 \times R + 48{,}477 \quad (4)$$

Where, $T_{col}(R)$ is the collector's temperature corresponding to radius R. R : collector's radius, 10 cm ≤R≤50 cm.

Similarly, the absorber temperature (T_{abs}) decreases progressively with increasing radius (R), as illustrated in Figure 2(b). For instance, the temperature at point 4 (D=18.75 cm) was 59.1 °C, while at point 2 (D=38.75 cm), it was 57.1 °C. An increase in radius of 20 cm corresponds to a 2 °C decrease in temperature, representing a 1.96% relative reduction. This linear decrease in temperature along the absorber radius is well described by a linear model with a coefficient of determination ($R^2 = 0.957$), defined by the following formula:

$$T_{abs}(R) = -0{,}0658 \times R + 60{,}33 \quad (5)$$

Where, $T_{abs}(R)$ is the absorber's temperature corresponding to radius R. R : Absorber's radius, 10 cm ≤R≤50 cm

The absorber temperatures are higher than those of the collector due to the greater amount of heat absorbed, which is directly related to incident solar radiation. Likewise, the rate of temperature decrease with radius R is more pronounced on the absorber (−0.0929 °C/cm) than on the collector (−0.0658 °C/cm), indicating that absorber temperatures vary more strongly with airflow direction. Both the absorber and collector contribute to increasing the air temperature, implying that air temperature rises as the diameter R of either component decreases, consistent with findings reported in the literature (Abdelsalam et al., 2024, Dai et al., 2003).

Prolonged exposure of the absorber to solar radiation elevates its temperature, which in turn heats the air via conduction and convection. This movement generates a longitudinal thermal gradient, as the air entering the collector is relatively cooler. In accordance with the principle of mass conservation, the air velocity at the chimney inlet increases when the diameter decreases, enhancing the transport of thermal energy and improving the overall efficiency of the system.

4.2 Effect of operatonal conditions on the collector temperature for each raduis

The evolution of collector temperature at the five measurement points (1–5) as a function of solar radiation (G) and ambient temperature (T_{amb}) is presented in Figure A1 (a and b). It is evident that increases in both G and T_{amb} result in higher temperatures at all collector points. The effects of these parameters were captured using second-order polynomial models for each point, summarized in Table 1. The coefficients of determination (R^2) for the individual effects of GGG and T_{amb} range from 0.955 to 0.971 and from 0.944 to 0.971, respectively.

A combined polynomial model was then developed for each point to describe collector temperature as a function of both G and T_{amb} simultaneously, implemented in MATLAB. The resulting models, also listed in Table 1, exhibit high goodness-of-fit with R^2 values ranging from 0.973 (point 2) to 0.989 (point 4). The uncertainties of the moel coefficients were evaluated using standard errors from nonlinear regression, and 95% confidence intervals indicate that all coefficients are statistically significant ($p<0.05$). These results confirm the robustness of the two-variable polynomial models for accurately describing collector temperatures at different locations.

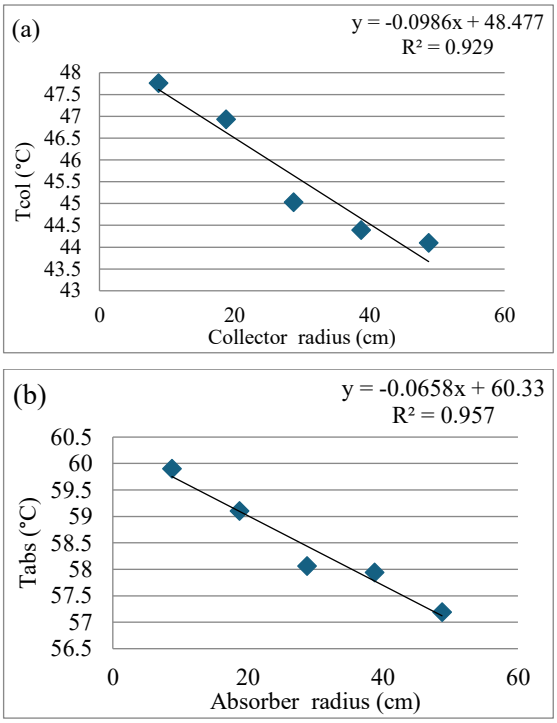

Figure 2. Temperature evolution along the radius of the collector (a) and absorber (b).

4.3 Effect of operatonal conditions on the absorber temperature for each raduis

Figure A2 shows the evolution of absorber temperature (T_{abs}) at five points (1–5) as a function of solar radiation (G) and ambient temperature (T_{abs}). As observed, increases in solar radiation and ambient temperature lead to higher absorber temperatures, which are well captured by second-order polynomial models. Table 2 summarizes these models, describing T_{abs} at each point as a function of G and T_{abs} . The uncertainties of the model coefficients were evaluated using standard errors from nonlinear regression, and 95% confidence intervals indicate that all coefficients are statistically significant ($p<0.05$), confirming the robustness of the fit. The absorber temperature rises nonlinearly with both solar radiation intensity and ambient temperature. As solar radiation increases, the absorber stores more thermal energy, though part of this energy is simultaneously lost through convection and radiation. The polynomial model captures this balance between energy input and thermal dissipation. Consequently, the temperature rise enhances the air flow rate through the collector, due to the temperature difference between the collector inlet and outlet, improving thermal energy transfer to the circulating air and thereby increasing the overall efficiency of the solar chimney system. Consistent with Ihaddadene et al., 2025, higher collector and absorber temperatures raise the air temperature and velocity, which in turn increases the mass flow rate, ultimately improving the performance of the solar chimney in terms of both efficiency and power output.

Table 1. The mathematical models of Tcol at each point as a function of G and T_{amb}.

.	Effect of solar radiation		Effect ambient temperature	
Point1	$T_{1col} = -4 \times 10^{-5} \times G^2 + 0{,}0823 \times G + 0{,}5353$ (R^2=0,971)	(6)	$T_{1col} = -0{,}1621 \times Tamb^2 + 10{,}477 \times Tamb - 126{,}12$ (R^2=0,947)	(11)
Point2	$T_{2col} = -4 \times 10^{-5} \times G^2 + 0{,}0822 \times G + 1{,}8308$ (R^2=0,955)	(7)	$T_{2col} = -0{,}1557 \times Tamb^2 + 10{,}077 \times Tamb - 119{,}13$ (R^2=0,944)	(12)
Point3	$T_{3col} = -4 \times 10^{-5} \times G^2 + 0{,}0856 \times G + 0{,}7142$ (R^2=0,956)	(8)	$T_{3col} = -0{,}1745 \times Tamb^2 + 11{,}188 \times Tamb - 134{,}78$ (R^2=0,956)	(13)
Point4	$T_{4col} = -4 \times 10^{-5} \times G^2 + 0{,}1001 \times G - 4{,}4188$ (R^2=0,961)	(9)	$T_{4col} = -0{,}1859 \times Tamb^2 + 12{,}014 \times Tamb - 147{,}99$ (R^2=0,971)	(14)
Point5	$T_{5col} = -4 \times 10^{-5} \times G^2 + 0{,}1021 \times G - 4{,}5723$ (R^2=0,964)	(10)	$T_{5col} = -0{,}2043 \times Tamb^2 + 13{,}039 \times Tamb - 161{,}4$ (R^2=0,966)	(15)
Effects of G et T_{amb} at the same time				
Point1	$T_{1col} = -0{,}0434 \times {T_{amb}}^2 - 1{,}885 \times 10^{-5} \times G^2 + 3{,}003 \times T_{amb} + 0{,}04328 \times G - 32{,}21$($R^2$=0,9841)			(16)
Point2	$T_{2col} = -0{,}05408 \times {T_{amb}}^2 - 1{,}608 \times 10^{-5} \times G^2 + 3{,}675 \times T_{amb} + 0{,}03699 \times G - 38{,}66$ (R^2=0,9726)			(17)
Point3	$T_{3col} = -0{,}08169 \times {T_{amb}}^2 - 1{,}149 \times 10^{-5} \times G^2 + 5{,}311 \times T_{amb} + 0{,}02983 \times G - 59{,}43$ (R^2=0,9838)			(18)
Point4	$T_{4col} = -0{,}1053 \times {T_{amb}}^2 - 0{,}9329 \times 10^{-5} \times G^2 + 6{,}904 \times T_{amb} + 0{,}0251 \times G - 82{,}09$ (R^2=0,9887)			(19)
Point5	$T_{5col} = -0{,}0967 \times {T_{amb}}^2 - 1{,}429 \times 10^{-5} \times G^2 + 6{,}421 \times T_{amb} + 0{,}03314 \times G - 76{,}94$ (R^2=0,9858)			(20)

Table 2. The mathematical models of Tabs at each point as a function of G and T_{amb}.

	Effect of solar radiation		Effect ambient temperature	
4	$T_{1abs} = -7 \times 10^{-5} \times G^2 + 0{,}1398 \times G - 9{,}8984$ (R^2=0,964)	(21)	$T_{1abs} = -0{,}3378 \times Tamb^2 + 0{,}614 \times Tamb - 258{,}42$ (R^2=0,956)	(26)
Point2	$T_{2abs} = -7 \times 10^{-5} \times G^2 + 0{,}1338 \times G - 6{,}347$ (R^2=0,935)	(22)	$T_{2abs} = -0{,}3564 \times Tamb^2 + 21{,}391 \times Tamb - 265{,}46$ (R^2=0,941)	(27)
Point3	$T_{3abs} = -7 \times 10^{-5} \times G^2 + 0{,}1365 \times G - 7{,}2832$ (R^2=0,954)	(23)	$T_{3abs} = -0{,}3745 \times Tamb^2 + 22{,}518 \times Tamb - 281{,}64$ (R^2=0,953)	(28)
Point4	$T_{4abs} = -8 \times 10^{-5} \times G^2 + 0{,}1536 \times G - 13{,}617$ (R^2=0,962)	(24)	$T_{4abs} = -0{,}3846 \times Tamb^2 + 23{,}244 \times Tamb - 293{,}62$ (R^2=0,962)	(29)
Point5	$T_{5abs} = -6 \times 10^{-5} \times G^2 + 0{,}1245 \times G - 3{,}2095$ (R^2=0,970)	(25)	$T_{5abs} = -0{,}3064 \times Tamb^2 + 18{,}938 \times Tamb - 234{,}46$ (R^2=0,951)	(30)
Effects of G et T_{amb} at the same time				
Point1	$T_{1abs} = -0{,}1928 \times {T_{amb}}^2 - 2{,}829 \times 10^{-5} \times G^2 + 11{,}54 \times T_{amb} + 0{,}05933 \times G - 147$ (R^2=0,9787)			(31)
Point2	$T_{2abs} = -0{,}2298 \times {T_{amb}}^2 - 2{,}509 \times 10^{-5} \times G^2 + 13{,}48 \times T_{amb} + 0{,}05227 \times G - 168{,}5$ (R^2=0,9619)			(32)
Point3	$T_{3abs} = -0{,}2368 \times {T_{amb}}^2 - 2{,}436 \times 10^{-5} \times G^2 + 13.86 \times T_{amb} - 0{,}05334 \times G - 174.1$ (R^2=0,9788)			(33)
Point4	$T_{4abs} = -0{,}221 \times {T_{amb}}^2 - 3.35 \times 10^{-5} \times G^2 + 13.19 \times T_{amb} - 0{,}06662 \times G - 171.1$ (R^2=0,9835)			(34)
Point5	$T_{5abs} = -0{,}1704 \times {T_{amb}}^2 - 1.849 \times 10^{-5} \times G^2 + 10.29 \times T_{amb} + 0{,}04544 \times\times G - 123.5$ (R^2=0,9761)			(35)

4.4 The generalized model governing the thermal behavior of the collector and absorber

The generalized model for the collector temperature evaluates the temperature at different points (1, 2, 3, 4, and 5) as a function of solar radiation, ambient temperature, and position, as noted in Section 3. This model is illustrated by Equation 37.

$$T_{col}(G, T_{amb}, x) = a_{col}(x) \times G^2 + b_{col}(x) \times G + c_{col}(x) \times {T_{amb}}^2 + d_{col}(x) \times T_{amb} + e_{col}(x) \quad (37)$$

The coefficients ($a_{col}(x)$, $b_{col}(x)$, $c_{col}(x)$, $d_{col}(x)$, and $e_{col}(x)$) are functions of the collector radius (position xxx). They were determined by fitting fourth-order polynomials to the local regression coefficients obtained from the five measured points, using MATLAB software. All terms were statistically significant ($p < 0.05$), indicating the robustness of the generalized model.

$$a_{col}(x) = -1.85 \times 10^{-12} \times x^4 + 9{,}57 \times 10^{-10} \times x^3 - 8{,}541 \times 10^{-8} \times x^2 + 2{,}2996 \times 10^{-6} \times x - 2{,}85 \times 10^{-5} (R^2 = 1) \quad (38)$$

$$b_{col}(x) = 3{,}033 \times 10^{-8} \times x^4 - 7{,}583 \times 10^{-6} \times x^3 + 5{,}206 \times 10^{-4} \times x^2 - 0{,}01104 \times x - 0.03503 \quad (R^2 = 1) \tag{39}$$

$$c_{col}(x) = 2{,}933 \times 10^{-8} \times x^4 - 4{,}51 \times 10^{-6} \times x^3 - 2{,}527 \times 10^{-4} \times x^2 - 5{,}429 \times 10^{-3} \times x - 0{,}06414 \quad (R^2 = 1) \tag{40}$$

$$d_{col}(x) = -4{,}275 \times 10^{-6} \times x^4 + 7{,}454 \times 10^{-4} \times x^3 - 0{,}04284 \times x^2 + 0{,}8385 \times x + 1{,}916 \quad (R^2 = 1) \tag{41}$$

$$e_{col}(x) = 7{,}421 \times 10^{-5} \times x^4 - 0.01204 \times x^3 + 0{,}6531 \times x^2 - 12.22 \times x - 12.42 \quad (R^2 = 1) \tag{42}$$

The same methodology was applied to determine the absorber temperatures at any position. The resulting generalized model for the absorber temperature is expressed by the following equations:

$$T_{abs}(G, T_{amb}, x) = a_{abs}(x) \times G^2 + b_{abs}(x) \times G + c_{abs}(x) \times {T_{abs}}^2 + d_{abs}(x) \times T_{abs} + e_{abs}(x) \tag{43}$$

The coefficients $a_{abs}(x)$, $b_{abs}(x)$, $c_{abs}(x)$, $d_{abs}(x)$ and $e_{abs}(x)$ are functions of the absorber radius (position). They were determined by fitting fourth-order polynomial functions to the local regression values obtained from the five measurement points using MATLAB. All coefficients were statistically significant ($p < 0.05$), confirming the reliability and robustness of the generalized model.

$$a_{abs}(x) = 1{,}716 \times 10^{-10} \times R^4 - 2{,}195 \times 10^{-8} \times R^3 + 9{,}762 \times 10^{-7} \times R^2 - 1{,}737 \times 10^{-5} \times R + 7{,}243 \times 10^{-5} (R^2 = 1) \tag{44}$$

$$b_{abs} = 8{,}5 \times 10^{-8} \times R^4 - 1{,}017 \times 10^{-5} \times R^3 + 5{,}595 \times 10^{-4} \times R^2 - 0{,}01542 \times R - 0{,}07197 \quad (R^2 = 1) \tag{45}$$

$$c_{abs}(x) = -2.13 \times 10^{-7} \times R^4 + 2{,}803 \times 10^{-5} \times R^3 + 1{,}279 \times 10^{-4} \times R^2 + 2.319 \times 10^{-3} \times R - 0{,}07717 \quad (R^2 = 1) \tag{46}$$

$$d_{abs(x)} = -7{,}042 \times 10^{-6} \times R^4 + 8{,}656 \times 10^{-4} \times R^3 - 0{,}04428 \times R^2 + 1{,}078 \times R + 3{,}709 \quad (R^2 = 1) \tag{47}$$

$$e_{abs}(x) = 1{,}904 \times 10^{-4} \times x^4 - 0.02439 \times x^3 + 1{,}18 \times x^2 - 25.07 \times x + 20.76 \; (R^2 = 1) \tag{48}$$

To validate the generalized collector and absorber temperature models, a statistical analysis was performed using four indicators: the coefficient of determination (R^2), the root mean square error (RMSE), the normalized root mean square error (NRMSE), and the Nash–Sutcliffe efficiency (NSE). The NSE is widely used in modeling within hydrological, thermal, and climatic studies. Both NSE and R^2 are statistical measures that assess the quality of a model's fit to experimental data. While they share similar mathematical formulations, their interpretations differ: an NSE of 1 indicates a perfect model, values greater than 0.75 denote excellent performance, and values below 0 indicate that the model performs worse than the mean. The mathematical expressions for these indicators are presented in the following equations:

$$R^2 = 1 - \frac{\sum_{i=1}^{n}(T_{i,exp} - T_{i,mod})}{\sum_{i=1}^{n}(T_{i,exp} - \overline{T_{i,mod}})} \tag{49}$$

$$RMSE = \sqrt{\frac{1}{n}\left(\sum_1^n (T_{i,exp} - T_{i,mod})\right)^2} \tag{50}$$

$$NRMSE = \frac{\sum_i^n (T_{i,exp} - T_{i,mod})^2}{\sum_i^n {T_{i,exp}}^2} \tag{51}$$

Where, n : The number of values during the experiment, $T_{i,exp}$: The experimental temperature of point i in the collector (or in the absorber), $T_{i,exp}$: The calculated temperature by the global model of point i in the collector (or in the absorber), $\overline{T_{i,mod}}$: The average temperature of the model in the collector (or in the absorber).

Statistical evaluation of the generalized collector (Tcol) and absorber (Tabs) temperatures was conducted to assess the performance of the generalized models. Table 3 summarizes the statistical indicators for both the collector and the absorber at the different measurement points. The generalized model accurately predicts the collector temperature at each point, as evidenced by high coefficients of determination (R^2), ranging from 0.973 (Tcol2) to 0.989 (Tcol4), low RMSE values between 0.510°C (Tcol4) and 0.9823°C (Tcol5), and low NRMSE values from 0.0143% (Tcol4) to 0.0515% (Tcol5). Similarly, all NSE values exceed 0.75, confirming that the generalized model performs at an excellent level.

Similar results were observed for the generalized absorber (Tabs) model. As shown in Table 3, the model exhibits high R^2 values, ranging from 0.962 (point 2) to 0.983 (point 4), low RMSE values between 0.7678°C (point 4) and 1.189°C (point 1), and NRMSE values from 0.019% (point 4) to 0.05% (point 1). All NSE values exceed 0.75, confirming that the generalized absorber model performs at an excellent level.

Another validation approach involved comparing the generalized model predictions with experimental data for both the collector and absorber. Figure 3 presents the comparison between the experimental collector temperatures at the five measurement points and the temperatures predicted by the generalized model. The results demonstrate a strong agreement across all points, with minimal deviations. This close alignment confirms that the generalized polynomial formulation reliably captures the thermal behavior of the collector as a function of solar radiation, ambient temperature, and spatial position.

Figure 4 shows the comparison between the generalized absorber model and the experimental data. The results indicate that the generalized model closely fits the experimental measurements. Statistical analysis of all data points (five on the collector and five on the absorber) is presented in Table 3. The generalized models exhibit high accuracy, with R^2 values of 0.9802 for the collector and 0.9739 for the absorber, RMSE around 0.7, NRMSE of 0.0194 (collector) and 0.0174 (absorber), and NSE values greater than 0.79. These results confirm that the generalized absorber model reliably reproduces the observed thermal behavior, with minimal deviations, validating the robustness of the polynomial formulation for estimating absorber temperatures as a function of solar radiation, ambient temperature, and spatial position.

Table 3. The statistical indices of the global models of Tcol and Tabs at each point.

Point	R^2	RMSE	NRMSE	NSE	Point	R^2	RMSE	NRMSE	NSE
T1col	0,9840	0,6810	0,0289	0,9840	T1abs	0,9786	1,189	0,050	0,9786
T2col	0,9726	0,6944	0,0289	0,9726	T2abs	0,9619	1,074	0,041	0,9619
T3col	0,9838	0,5473	0,0174	0,9838	T3abs	0,9788	0,849	0,0249	0,9788
T4col	**0,9887**	**0,5097**	**0,0143**	**0,9887**	T4abs	**0,9834**	**0,7678**	**0,0192**	**0,9834**
T5col	0,9838	0.9823	0,0515	0,9838	T5abs	0,9761	0,8664	0,0253	0,9761
Tcol	0.9802	0.70	0.0194	**0.9802**	Tabs	0.9739	0.9623	0.0174	**0.9739**

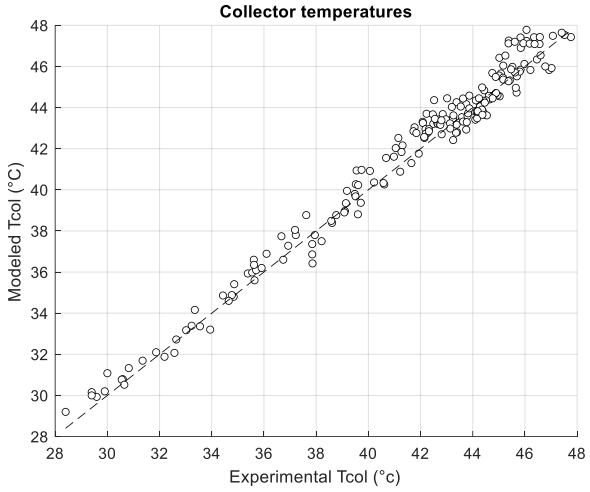

Figure 3. Comparison of collector temperatures (experimental and modeled) at different points (1, 2, 3, 4 and 5).

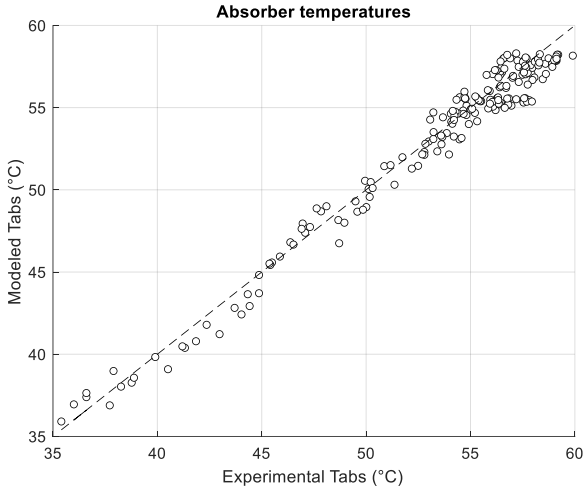

Figure 4. Comparison of absorber temperatures (experimental and modeled) at different points (1, 2, 3, 4 and 5).

5. CONCLUSIONS

The performance of a solar chimney is influenced by multiple factors, including geometric parameters and climatic conditions, with solar radiation and ambient temperature being the most critical. This experimental study focuses on modeling the thermal behavior of the collector and absorber in a small solar chimney prototype. Temperatures were recorded at five positions on the collector and five positions on the absorber under varying solar radiation and ambient temperature. These measurements were used to develop local models for the collector and absorber using second-order polynomial regression in solar radiation and ambient temperature for each point. A generalized model was then constructed, expressing collector and absorber temperatures as continuous functions of spatial position through fourth-order polynomial functions of the radius.

Key findings include:

- Collector and absorber temperatures increase as the radius decreases, following a linear relationship with coefficients of determination $R^2 = 0.929$ (collector) and $R^2 = 0.957$ (absorber).
- Collector temperatures at each location are strongly influenced by solar radiation and ambient temperature, with local second-order polynomial models yielding R^2 values between 0.973 and 0.989.
- Absorber temperatures are similarly affected, with R^2 values between 0.9619 and 0.9835 for local polynomial models.
- The main contribution of this work is the generalization of the collector and absorber thermal profiles. Instead of treating discrete points independently, a continuous model predicts temperature at any location along the collector or absorber as a function of solar radiation, ambient temperature, and spatial position. This addresses a gap in existing literature, where spatial variability is often neglected.

The generalized models were validated using four statistical indices (R^2, RMSE, NRMSE, and NSE), showing strong agreement with experimental data: collector model (R^2 = 0.9802, NRMSE = 0.0194, NSE = 0.98) and absorber model (R^2 = 0.974, NRMSE = 0.0174, NSE = 0.974). These results demonstrate the models' reliability and potential for solar system simulations and thermal optimization. Future work will extend the model to predict air temperature between the absorber and collector and compare results with numerical simulations using ANSYS.

6. ACKNOWLEDGEMENT

The authors would like to thank Saadi Ibrahim and Abahri Athmane for their help during the realization of the experimental part.

NOMENCLATURE

G	Solar radiation (W/m²)
n	Number of values during the experiment
R	collector's (absorber's) radius (cm)
T	Temperature (°C)
R^2	Coefficient of determination
RMSE	Root mean square error
NRMSE	Normal Root Mean Square Error
NSE	Nash–Sutcliffe efficiency

Greek letters

-	-

Subscripts

abs	Absorber
amb	Ambiante
col	Collector
i,exp	The experimental value of point i in the collector (or in the absorber)
i,mod	The modeled value of point i in the collector (or in the absorber)

Appendix

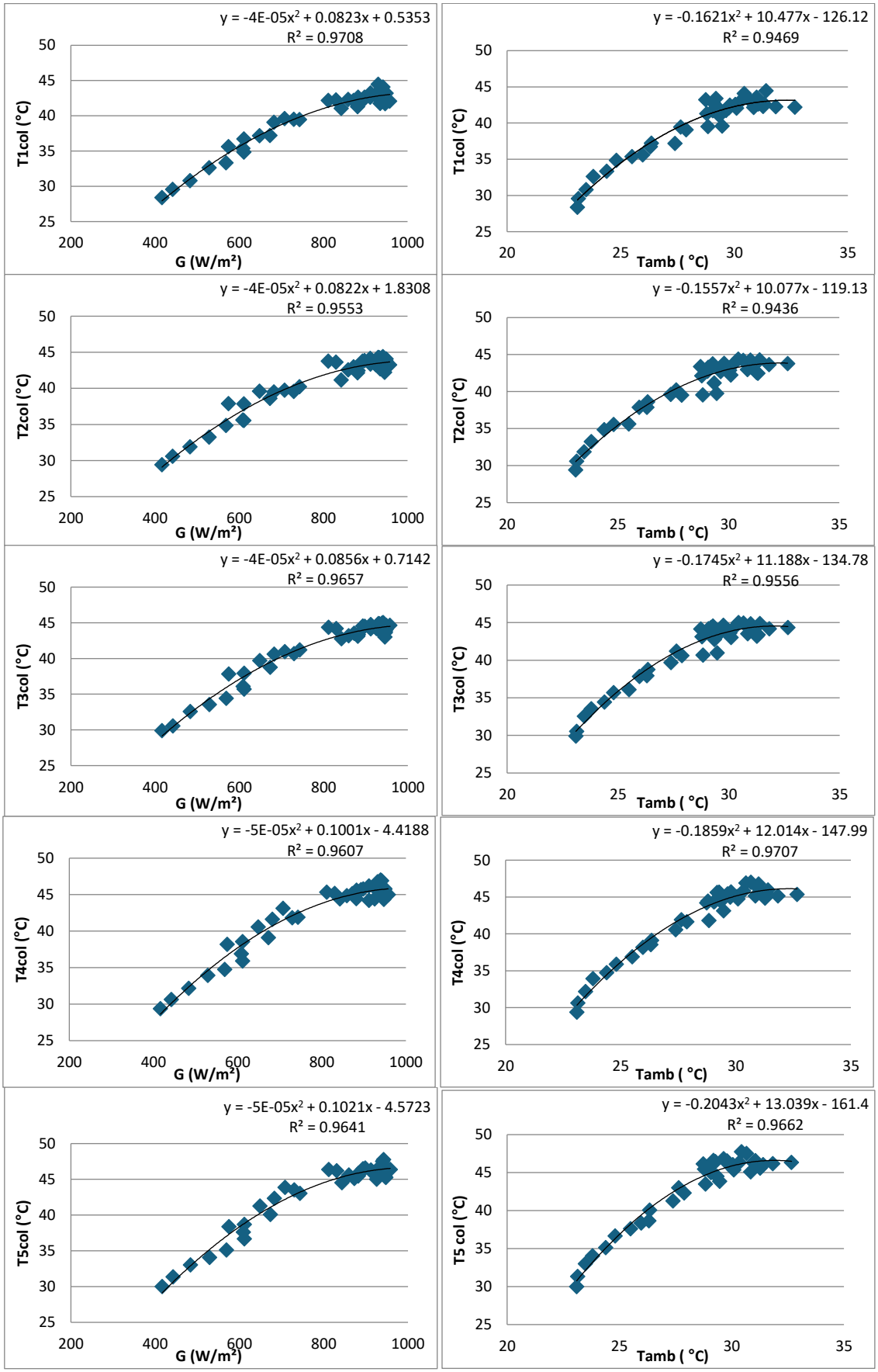

(a) (b)

Figure A1. Temperature evolution of collector points 1, 2, 3, 4, and 5 as a function of solar radiation (G) (a) and ambient temperature (T_{amb}) (b).

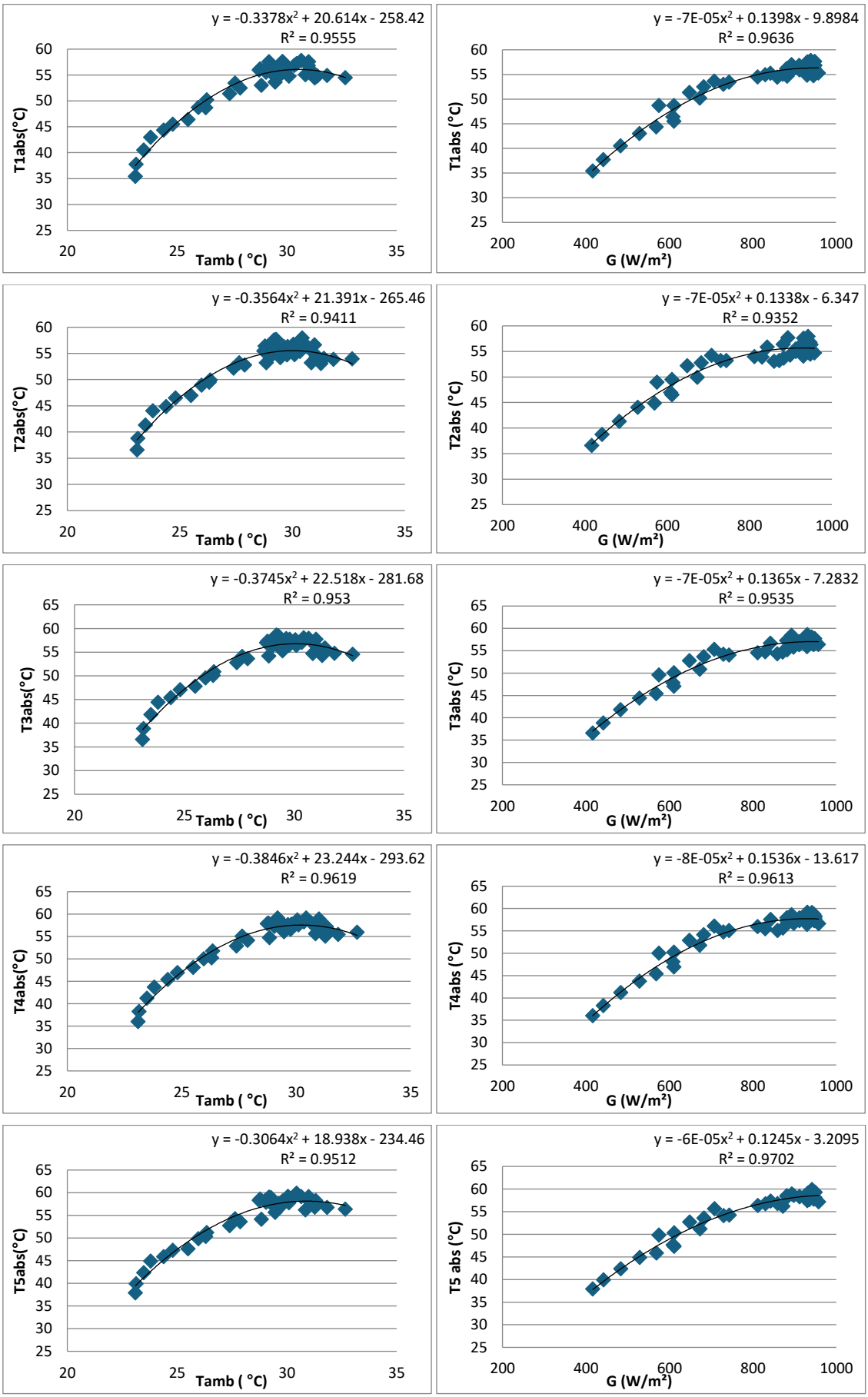

(a) (b)

Figure A2. Temperature evolution of absorber points 1, 2, 3, 4, and 5 as a function of solar radiation (G) (a) and ambient temperature (T_{amb}) (b).

REFERENCES

1. Abdelsalam, E., Almomani, F., Hamza A., Dareen, H., Mohammad, J. (2024). Sustainable production of green hydrogen, electricity, and desalinated water via a Hybrid Solar Chimney Power Plant (HSCPP) water-splitting process. *International Journal of Hydrogen Energy*. 52B, 1356-1369. https://doi.org/10.1016/j.ijhydene.2023.06.165
2. Abdelsalam, E., Almomani, F., Ibrahim, S., Kafiah, F., Jamjoum, M., Alkasrawi, M. (2023). A Novel Design of a Hybrid Solar Double-Chimney Power Plant for Generating Electricity and Distilled Water. *Sustainability*,15, 2729. https://doi.org/10.3390/su15032729
3. Abuashe, I. A., Mariamy, A. M.(2024). Minimizing the size of large-scale solar chimney power plant. *Malaysian Journal of Industrial Technology (MJIT)*, 8(1), eISSN: 2637-1081. https://mitec.unikl.edu.my/wp-content/uploads/2024/03/2-MINIMIZING-THE-SIZE-OF-LARGE-SCALE-SOLAR-CHIMNEY-POWER-PLANT.pdf
4. Aliaga, D.M., Feick, R., Brooks, W.K., Mery, M., Gers, R., Levi, J.F., Romero, C.P.(2021). Modified Solar Chimney Configuration with a Heat Exchanger: Experiment and CFD Simulation. *Therm. Sci. Eng. Prog*, *22*, 100850. https://doi.org/10.1016/j.tsep.2021.100850
5. Alkasrawi, M.. Abdelsalam, E., Alnawafah, H., Almomani, F., Tawalbeh, M., Mousa, A. (2021). Integration of Solar Chimney Power Plant with Photovoltaic for Co-Cooling, Power Production, and Water Desalination. *Processes*, *9*, 2155. https://doi.org/10.3390/pr9122155
6. Ayad T. Mustafa, Hussain H. Al-Kayiem, and Syed Ihtsham U. Gilani. (2015). Investigation and evaluation of the solar air collector model to support the solar vortex engine, *ARPN Journal of Engineering and Applied Sciences*, 10(12). http://www.arpnjournals.com/jeas/research_papers/rp_2015/jeas_0715_2247.pdf
7. Ayadi, A., Bouabidi, A., Driss, Z., Abid, M.S. (2018a). Experimental and numerical analysis of the collector roof height effect on the solar chimney performance. *Renew. Energy,* 115: 649–662. https://doi.org/10.1016/j.renene.2017.08.099
8. Ayadi, A., Driss, Z., Bouabidi, A., Nasraoui, H., Bsisa, M., Abid, M.S.(2018b). A computational and an experimental study on the effect of the chimney height on the thermal characteristics of a solar chimney power plant. *Proceedings of the Institution of Mechanical Engineers, Part E: Journal of Process Mechanical Engineering*, 232(4): 503-516. https://doi.org/10.1177%2F0954408917719776
9. Ayli, U.E., Özgirgin, E., and Tareq, M. (2021). Solar Chimney Power Plant Performance for Differen Seasons Under Varying Solar Irradiance and Temperature Distribution. *Journal of Energy Resources Technology*, 143(6). https://doi.org/10.1115/1.4048533
10. Cuce, E., Cuce, P.M., Sen, H., Sudhakar, K., Berardi, U., Serencam, U. (2021). Impacts of ground slope on main performance figures of solar chimney power plants: A comprehensive CFD research with experimental validation. *Int. J. Photoenergy*, 6612222. https://doi.org/10.1155/2021/6612222
11. Cuce, P.M.,. Saxena, A,. Cuce, E., Kontoleon, K. J., Oztekin E.K., Shaik, S., and Guo, S. (2024). Thermal and energy analysis of a novel solar updraft tower design with divergent chimney and convergent collector concept: CFD analysis with experimental validation. *International Journal of Low-Carbon Technologies*, 19, 714–722. https://academic.oup.com/ijlct/article/doi/10.1093/ijlct/ctad152/7636622
12. Dai, Y. J., Huang, H. B., & Wang, R. Z. (2003). Case study of solar chimney power plants in Northwestern regions of China. *Renewable energy*, 28(8), 1295-1304. https://doi.org/10.1016/S0960-1481(02)00227-6
13. Ghalamchi, M., Kasaeian, A., Ghalamchi, M., Mirzahosseini, A.H. (2016). An experimental study on the thermal performance of a solar chimney with different dimensional parameters. *Renew. Energy,*91: 477–483. https://doi.org/10.1016/j.renene.2016.01.091
14. Habibollahzade, A., Houshfar, E., Ashjaee, M., Behzadi, A., Gholamian, E., Mehdizadeh, H.(2018). Enhanced Power Generation through Integrated Renewable Energy Plants: Solar Chimney and Waste-to-Energy. *Energy Convers. Manag,*166, 48–63. https://doi.org/10.1016/j.enconman.2018.04.010
15. Hamdan, M.O. (2013). Analysis of solar chimney power plant utilizing chimney discrete model. *Renew. Energy*; 56 :50-54. https://doi.org/10.1016/j.renene.2012.09.047
16. Hassan, A., Ali, M., Waqas, A. (2018). Numerical investigation on performance of solar chimney power plant by varying collector slope and chimney diverging angle. *Energy*, 142, 411–425. https://doi.org/10.1016/j.energy.2017.10.047
17. https://ec.europa.eu/eurostat/data
18. https://ember-energy.org/latest-insights/eu-wind-and-solar-overtake-fossil-fuels/#wind-and-solar-overtake-fossil-fuels
19. https://www.irena.org//media/Files/IRENA/Agency/Publication/2024/Mar/IRENA_RE_Capacity_Statistics_2024.pdf?rev=a587503ac9a2435c8d13e40081d2ec34
20. https://www.irena.org/Publications/2024/Mar/Renewable-capacity-statistics-2024
21. Ihaddadene, R., Ihaddadene, N., Bedjeghit, E., Semane, A., Guerira, B. (2025). Study of the variation of temperatures in a solar chimney. *Sigma Journal of Engineering and Natural Sciences,* 43 (1),1-10. https://doi.org/10.14744/sigma.2024.00111
22. Ihaddadene, R., Ihaddadene, N., and Guerira, B. A simulation study of the impact of solar radiation on the solar chimney. 2nd International Conference on Engineering, Natural and Social Sciences. April 4-6, 2023 : Konya, Turkey. https://drive.google.com/file/d/18dZW7hluqakAQuWHlWZs1TnfiBiroGeB/view
23. Karimipour-Fard, P., & Beheshti, H. (2017). Performance enhancement and environmental impact analysis of a solar chimney power plant: Twenty-four-hour simulation in climate condition of isfahan province, iran. *International Journal of Engineering*, *30*(8), 1260-1269. https://www.ije.ir/article_73005.html
24. Kasaeian, A., Ghalamchi, M., Ghalamchi, M. (2014). Simulation and optimization of geometric parameters of a solar chimney in Tehran. *Energy Convers. Manag,* *83*:28–34. https://doi.org/10.1016/j.enconman.2014.03.042
25. Larbi, S., Bouhdjar, A., & Chergui, T. (2010). Performance analysis of a solar chimney power plant in the southwestern region of Algeria. *Renewable and Sustainable energy reviews,* 14(1), 470-477. https://doi.org/10.1016/j.rser.2009.07.031
26. Mokrani, O.B.E.K.; Ouahrani, M.R.; Sellami, M.H., Segni, L. (2020). Experimental Investigations of Hybrid: Geothermal Water/Solar Chimney Power Plant. *Energy Sources Part A Recovery Util. Environ. Eff.*,1–18. 10.1080/15567036.2020.1810830
27. Nasraoui, H., Driss, Z., Ayadi, A., Bouabidi, A., Kchaou, H.(2019). Numerical and experimental study of the impact of conical chimney angle on the thermodynamic characteristics of a solar chimney power plant. *Proc. Inst. Mech. Eng. Part E*, *233*, 1185–1199. https://doi.org/10.1177/0954408919859160
28. Patel, S.K., Prasad, D., Ahmed, M.R. (2014). Computational studies on the effect of geometric parameters on the performance of a solar chimney power plant. *Energy Convers. Manag*, 77: 424–431. https://doi.org/10.1016/j.enconman.2013.09.056
29. Sarthak, Mamgain., Shubham, Aggarwal., Meeta, Sharma., and Anoop, Kumar, Shukla.(2022). Recent perspectives and outlook of advances in technologies of solar chimney power plant. International Symposium on Fluids and Thermal Engineering (FLUTE 2021). *Journal of Physics: Conference Series* 2178 012009 IOP Publishing. https://doi.org/10.1088/1742-6596/2178/1/012009
30. Semane, A., Ihaddadene, R., Bedjeghit, E., Guerira, B., Ihaddadene, N.(2025). Experimental study of temperature changes in a solar chimney. *Journal of Thermal Engineering*, 11(2): 464-475. https://dx.doi.org/10.14744/thermal.0000927
31. Sen, H., Cuce, P.M., Cuce, E.(2021). Impacts of Collector Radius and Height on Performance Parameters of Solar Chimney Power Plants: A Case Study for Manzanares, Spain. *Recep Tayyip Erdogan University Journal of Science and Engineering,* 2(2): 83-104. https://doi.org/10.53501/rteufemud.1017909

32. Setareh, M. (2021). Comprehensive mathematical study on solar chimney power plant. *Renewable Energy,*175(C): 470-485. http://dx.doi.org/10.1016/j.renene.2021.05.017

33. Shahi, D.V.V., Gupta, M.A., Nayak, M.V.S.(2018). CFD Analysis of solar chimney wind power plant by Ansys Fluent. *Int. J. Technol. Res. Eng. 5*: 3746–3751. https://ijtre.com/wp-content/uploads/2021/10/2018050928.pdf

34. Sharon, H., Srinivas Reddy, K. (2024). Hybrid Solar Chimney-Thermal Desalination Systems. In: *Solar Thermal Desalination Technologies for Potable Water.* Springer, Cham. https://doi.org/10.1007/978-3-031-49155-9_11

35. Shuia, E.M., Arebi, B.H., and Abuashe, I.A. (2014). Experimental and Theoretical Investigation of Performance of a Solar Chimney Model, Part I: Experimental Investigation, *Solar Energy and Sustainable Development Journal*, 3(1): 51–62. https://doi.org/10.51646/jsesd.v3i1.88

36. Yapıcı, E., Özgirgin, A.E., and Osama, N. (2020). Numerical investigation on the performance of a small scale solar chimney power plant for different geometrical parameters. *Journal of Cleaner Production*, 276, https://doi.org/10.1016/j.jclepro.2020.122908

37. Zhou, X., Wang, F., Fan, J., & Ochieng, R.M. (2010). Performance of solar chimney power plant in Qinghai-Tibet Plateau. *Renewable and Sustainable energy reviews,* 14(8), 2249-2255. http://dx.doi.org/10.1016/j.rser.2010.04.017

38. Zou, Z., He, S. (2015). Modeling and Characteristics Analysis of Hybrid Cooling-Tower-Solar-Chimney System. *Energy Convers. Manag*, *95*, 59–68. https://doi.org/10.1016/j.enconman.2015.01.085